Using speckles to recover an image after its transmission through obstacles

Cleberson R. Alves, Alcenísio J. Jesus-Silva, and Eduardo J. S. Fonseca*
Instituto de Física, Universidade Federal de Alagoas, P.O. Box 2051, Maceió, AL, 57061-970, Brazil
(Received 19 October 2015; published 11 April 2016)

We show that an image, embedded into a speckle pattern, is robust against distortions during its transmission through obstacles. The robustness depends on the coherence length of the speckles and obstruction size. This behavior is based on the self-reconfiguration effect, where, even though some speckles have been blocked by an opaque obstacle, the speckle-pattern intensity is reestablished during propagation at the point where the signature of the obstacle disappears. We evaluated the self-reconfiguration ability of the image using the concepts of visibility and similarity.

DOI: 10.1103/PhysRevA.93.043816

I. INTRODUCTION

For a long time, scattering was considered only a detrimental effect that should be suppressed or avoided. However, recently, a series of interesting physical effects has been demonstrated and an enormous potential for disorder-based optical applications has been unveiled, ranging from fundamental optical studies to biomedical imaging. For instance, interesting effects have been explored with light possessing orbital angular momentum scattered by an opaque media such as spatial correlation singularity [1] and effective topological charge obtained from two partially coherent beams [2,3]. On the other hand, noninvasive imaging of a fluorescent object has been shown through a strongly scattering medium [4], with potential use in biomedical imaging [5]. And, recently, speckle correlation resolution enhancement has been proposed for high-resolution fluorescence imaging [6].

Scattering through an opaque media—such as biological tissue, glass, and plastic—carries spatial, temporal, and spectral information of the incident signal, and turns it into a speckle field. Therefore, if the incident wave is changed in any way, the speckle field changes accordingly. However, retrieving information from such field, getting information from the speckle pattern, or even controlling the light propagation have been a big challenge. For these purposes, several schemes have been presented [4,7–14].

In fact, currently there is a great interest to control both transmission and reflection of light by an opaque medium. Associated to that, the ability that some beams are capable of self-reconstructing or self-healing [15,16], even in the presence of massive particles, may offer new possibilities to look deeper into scattering tissues or to optimize an optical signal transmission through scattering media, for instance. Recently, two papers were published showing the importance of the self-healing coherent Bessel beams for microscopy [17,18], particularly for biological samples. At this point an interesting question arises: Is it possible, using a speckled beam as a light source, to recover an image after its transmission through an obstacle?

In this work, we show a remarkable property of speckles: the ability to image through obstacles. We demonstrate that it is possible to recover an image, without distortions, even when an obstacle is placed on its path. In fact, the insertion of an obstacle on the speckle field's path produces expressive changes in the speckle-pattern intensity. However, for a specific propagation distance, the obstacle signature disappears and whole image features are recovered. This fact is connected with the self-reconfiguration effect [19]. Additionally, another point explored in this work is that the recovery length along propagation depends on the spatial coherence length of the speckles and obstacle size. The image retrieval is evaluated using the concepts of visibility and similarity. A numerical simulation was used to support the experimental results and a theoretical analysis was presented as well.

II. EXPERIMENTAL SETUP

The experimental setup is shown schematically in Fig. 1. A Nd:YAG laser operating at 532 nm illuminates a computer generated hologram [20] with controllable pixels written in a Hamamatsu Model X10468-01 spatial light modulator (SLM) producing a Fourier transform of a Gaussian beam, as reference, and a Fourier transform of an image, namely the letter π, as a signal. Both beams were imaged over the scattering medium. A lens L_2 images the SLM over a rotating ground glass disk (RGGD) and L_3 is placed at a distance $f_3 =$ 140 mm from the RGGD. A circular pinhole (PH), placed at the focal plane of the lens L_2, was used to select the desired diffraction order. Some speckles were blocked by an obstacle and the transmitted ones were displayed in a charge-coupled device (CCD) camera for different longitudinal positions z. First, the reference beam was recorded by the CCD camera, and after that, the hologram was changed to acquire the signal beam. The RGGD, CCD camera, and SLM were synchronized to guarantee that the two acquired images are spatially incoherent but correlated between them. In fact, both signal and reference beams are scattered by the same region of the disk and detected one at a time by changing the hologram. Only after signal and reference measurements, the RGGD is rotated for the next set of measurements. To obtain two spatial coherence lengths of the speckles, we arrange the experimental setup for two different distances of d. For $d = 5$ cm, we have spatial coherence length of $\delta_1 = 31.1$ μm and for $d = 15$ cm, $\delta_2 = 17.7$ μm. This occurs because the spot size of the laser beam on the disk changes for different

*eduardo@fis.ufal.br

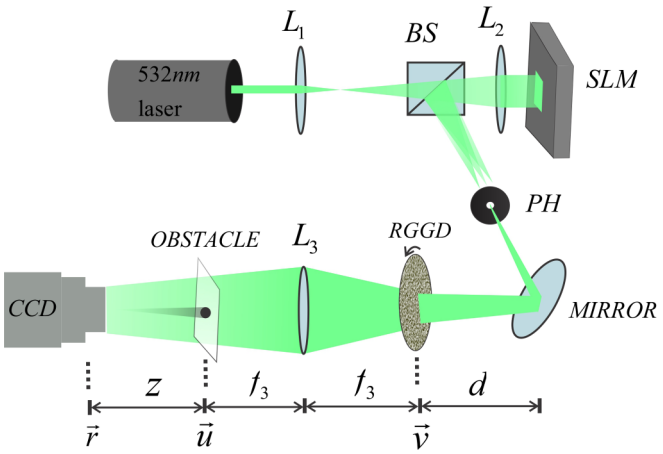

FIG. 1. Experimental setup. L_1, L_2, and L_3 are lenses with focal lengths $f_1 = 30$ mm, $f_2 = 300$ mm, and $f_3 = 140$ mm, respectively; BS: beam splitter; PH: pinhole; SLM: spatial light modulator; RGGD: rotating ground glass disk; and CCD: charge coupled device.

distances of d, and consequently, the spatial coherence length is changed accordingly. A numerical autocorrelation method was used to measure the spatial coherence length of the speckle [21]. The correlation curve possesses Gaussian distribution whose full width at half maximum gives the mean speckle size, which corresponds to the spatial coherence length of the speckle. Two obstacles were used with diameters of $D_1 \approx 2$ mm and $D_2 \approx 1$ mm. Each obstacle is a dark circle printed on a transparent sheet.

III. THEORETICAL ANALYSIS

The field propagation from the RGGD to the obstacle can be described by [22,23]

$$E_S(\vec{u}_1) = \int \exp\left(\frac{ik}{f_3}\vec{v}_1 \cdot \vec{u}_1\right)\tilde{\pi}(\vec{v}_1)G(\vec{v}_1)d^2v_1, \quad (1)$$

and

$$E_R(\vec{u}_2) = \int \exp\left(\frac{ik}{f_3}\vec{v}_2 \cdot \vec{u}_2\right)\tilde{g}(\vec{v}_2)G(\vec{v}_2)d^2v_2, \quad (2)$$

for the signal and reference beams, respectively. It is important to remember that these beams are speckle fields. k is the modulus of the wave vector and is given by $k = 2\pi/\lambda$, where λ is the wavelength. G describes the random effect of the RGGD. $\tilde{\pi}$ represents the Fourier transform of the image "π" and $\tilde{g}$ is a Fourier transform of a Gaussian beam.

The propagation from the obstacle to the CCD can be described by

$$E_S(\vec{r}_1) = \int \mathcal{O}(\vec{u}_1)E_S(\vec{u}_1)\exp\left[-\frac{i\pi}{\lambda z}(\vec{u}_1 - \vec{r}_1)^2\right]d^2u_1, \quad (3)$$

and

$$E_R(\vec{r}_2) = \int \mathcal{O}(\vec{u}_2)E_R(\vec{u}_2)\exp\left[-\frac{i\pi}{\lambda z}(\vec{u}_2 - \vec{r}_2)^2\right]d^2u_2, \quad (4)$$

where $\mathcal{O}$ represents the obstacle.

The field spatial correlation function at the detector points $\vec{r}_1$ and $\vec{r}_2$ is given by

$$\begin{aligned}\langle E_S(\vec{r}_1)E_R^*(\vec{r}_2)\rangle &= \left\langle \iint \mathcal{O}(\vec{u}_1)\mathcal{O}^*(\vec{u}_2)\exp\left[-\frac{i\pi}{\lambda z}(\vec{u}_1 - \vec{r}_1)^2\right.\right.\\ &\left.+\frac{i\pi}{\lambda z}(\vec{u}_2 - \vec{r}_2)^2\right]\left\{\iint \exp\left[\frac{ik}{f_3}(\vec{v}_1 \cdot \vec{u}_1 - \vec{v}_2 \cdot \vec{u}_2)\right]\right.\\ &\left.\left.\times \tilde{\pi}(\vec{v}_1)\tilde{g}^*(\vec{v}_2)G(\vec{v}_1)G^*(\vec{v}_2)d^2v_1d^2v_2\right\}d^2u_1d^2u_2\right\rangle. \quad (5)\end{aligned}$$

With sufficient scattering, the random effect of the GGD can be described by a Dirac delta function $\langle G(\vec{v}_1)G^*(\vec{v}_2)\rangle = \delta(\vec{v}_1 - \vec{v}_2)$. Therefore, the integrals in v_1 and v_2 in Eq. (5) become

$$\Gamma = \int \exp\left[\frac{ik}{f_3}\vec{v} \cdot (\vec{u}_1 - \vec{u}_2)\right]\tilde{\pi}(\vec{v})\tilde{g}^*(\vec{v})d^2v. \quad (6)$$

Considering that $\tilde{g}$ is the Fourier transform of a Gaussian with very narrow width, Eq. (6) is approximately the convolution of π with a Dirac delta function, resulting in

$$\Gamma = \pi(\vec{u}_1 - \vec{u}_2). \quad (7)$$

Inserting Eq. (7) into Eq. (5) and using the change of variables $\vec{u}_2 = \vec{u}_1 - \vec{u}$ and $\vec{r}_1 = \vec{r}$ and $\vec{r}_2 = 0$, we obtain

$$\begin{aligned}\langle E_S(\vec{r})E_R^*(0)\rangle = e^{-\frac{i\pi}{\lambda z}r^2}\iint \mathcal{O}(\vec{u}_1)\mathcal{O}(\vec{u}_1 - \vec{u})\\ \times \exp\left[-\frac{i2\pi}{\lambda z}\vec{u}_1 \cdot (\vec{u} - \vec{r})\right]\\ \times \exp\left(\frac{i\pi}{\lambda z}u^2\right)\pi(\vec{u})d^2u_1d^2u. \quad (8)\end{aligned}$$

It can be shown that, for any obstacle, the integral in the variable $\vec{u}_1$ in Eq. (8) results in a function which is approximately the Fourier transform of the obstacle function $\tilde{\mathcal{O}}(\vec{u} - \vec{r})$ which can be approximately described by a Dirac delta function $\tilde{\mathcal{O}}(\vec{u} - \vec{r}) \approx \delta(\vec{u} - \vec{r})$, such that

$$\begin{aligned}\langle E_S(\vec{r})E_R^*(0)\rangle &= e^{-\frac{i\pi}{\lambda z}r^2}\int \delta(\vec{u} - \vec{r})\exp\left(\frac{i\pi}{\lambda z}u^2\right)\pi(\vec{u})d^2u\\ &= \pi(\vec{r}). \quad (9)\end{aligned}$$

Based on Reed's momentum theorem [24], the correlation between the measured intensities $\langle I_S(\vec{r})I_R(0)\rangle$ is related to the modulus of the field correlation $|\langle E_S(\vec{r})E_R^*(0)\rangle|$ by

$$\langle I_S(\vec{r})I_R(0)\rangle - \langle I_S(\vec{r})\rangle\langle I_R(0)\rangle = |\langle E_S(\vec{r})E_R^*(0)\rangle|^2. \quad (10)$$

Thus, considering that the mean intensities at the measurement plane are uniform, the second term in Eq. (10) is just a constant background in the intensity correlation.

Looking at Eq. (9), it is clear that the π image was recovered after the obstacle $\mathcal{O}$. From the presented δ-correlated model the self-reconfiguration length [19] of the image is independent of z. However, in a more realistic scenario the function $\tilde{\mathcal{O}}(\vec{u} - \vec{r})$ is not a function of zero width. In this situation the size of π must be taken into account, and the π dimension depends on the spatial coherence length of the generated speckle fields.

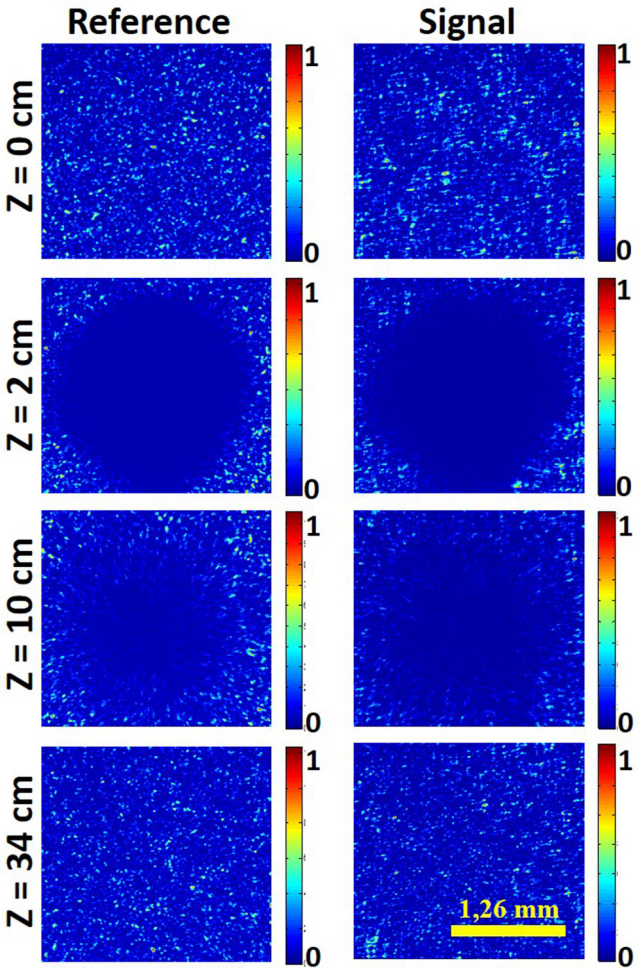

FIG. 2. Speckle patterns of the reference and signal beams measured for different distances of propagation, with spatial coherence length $\delta_1 = 33.1\ \mu$m and obstacle of diameter $D_1 \approx 2$ mm.

IV. RESULTS AND DISCUSSION

Figure 2 shows the reference and signal speckle-pattern intensities, with spatial coherence length of $\delta_1 = 31.1\ \mu$m, using matrices of 720×720 pixels corresponding to a region of 2.52 mm $\times$ 2.52 mm of the CCD camera. In the first line of Fig. 2, the CCD camera was placed at $z = 0$ cm. After measuring the speckle patterns, a transparent sheet with a dark circle of diameter $D_1 \approx 2$ mm was placed at $z = 0$ cm. From $z = 2$ cm to $z = 10$ cm, the obstacle signature is clearly observed. On the other hand, the entire speckle pattern becomes homogeneous or self-reconfigured [19] around $z =$ 34 cm.

The procedure used to obtain the result of cross correlation between the signal and reference speckle patterns was the following: We measured the reference intensity followed by the signal intensity, and, then, we numerically performed a cross correlation between them,

$$C(x,y) = \int_{-\infty}^{+\infty}\int_{-\infty}^{+\infty} I_S(x',y')I_R(x'-x,y'-y)dx'dy', \tag{11}$$

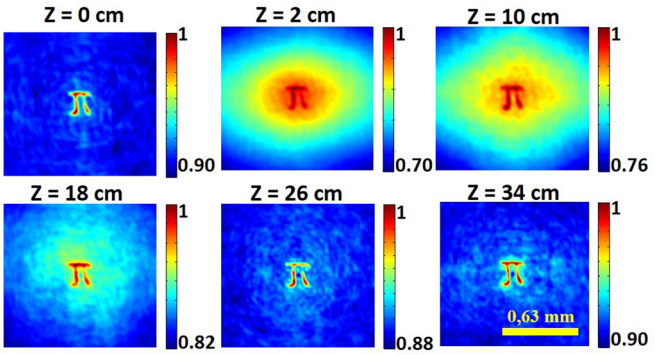

FIG. 3. Cross correlation between reference and signal beams for different distances of propagation, with coherence length $\delta_1 = 33.1\ \mu$m and obstacle of diameter $D_1 \approx 2$ mm.

where I_S and I_R are the signal and reference intensities, respectively. All experimental results presented in this work were averaged over 100 measurements.

The cross-correlation results between reference and signal of Fig. 2 are shown in Fig. 3. The first image (z = 0 cm) is exactly the retrieved image without obstacle. After that, a transparent sheet with an obstacle of diameter $D_1 \approx 2$ mm was placed on the speckles' path and a sequence of blurry images was measured. However, around $z = 34$ cm, the image π was clearly recovered. This position coincides with the self-reconfiguration of the speckles (see Fig. 2). We can see that all the details of the letter are recovered. Besides, the letter did not change its size along propagation because the speckle field is a collimated field. The speckles themselves do not change their size for the distance between the lens L_3 and the CCD camera position. We have used matrices of 360×360 pixels corresponding to a region of 1.26 mm $\times$ 1.26 mm of the CCD camera to display the images of Fig. 3.

The self-reconfiguration effect is characterized by having the same autocorrelation profile before and after the obstacle, as soon as the speckle-pattern intensity has been reconstructed [19]. The interesting point here is that the reconstruction of the letter π, which was obtained performing the cross-correlation procedure, coincides with the self-reconfiguration effect.

We can also observe in Fig. 3, through the color bars, that for $z = 2$ cm, the letter π is blurry and the obstacle signature has a strong influence on the image formation. However, during the propagation, and at $z = 34$ cm, the background increases, returning to the same level observed at $z = 0$ cm.

Figure 4 shows the reference and signal speckle-patterns intensity, for the same parameters as Fig. 2, but now with spatial coherence length of $\delta_2 = 17.7\ \mu$m. We observe that with the reduction of the spatial coherence length of the speckle, the obstacle effect disappears at a shorter distance, around $z = 17$ cm. Figure 5 shows the cross-correlation results between reference and signal of Fig. 4. We can clearly observe that the letter and the background are reestablished around $z = 17$ cm following Fig. 4.

Since Figs. 4 and 5 have the same dimensions as Figs. 2 and 3, respectively, comparing Fig. 5 with Fig. 3, we notice that the letter size has changed. This is observed because decreasing the spatial coherence length of the speckle, by increasing the

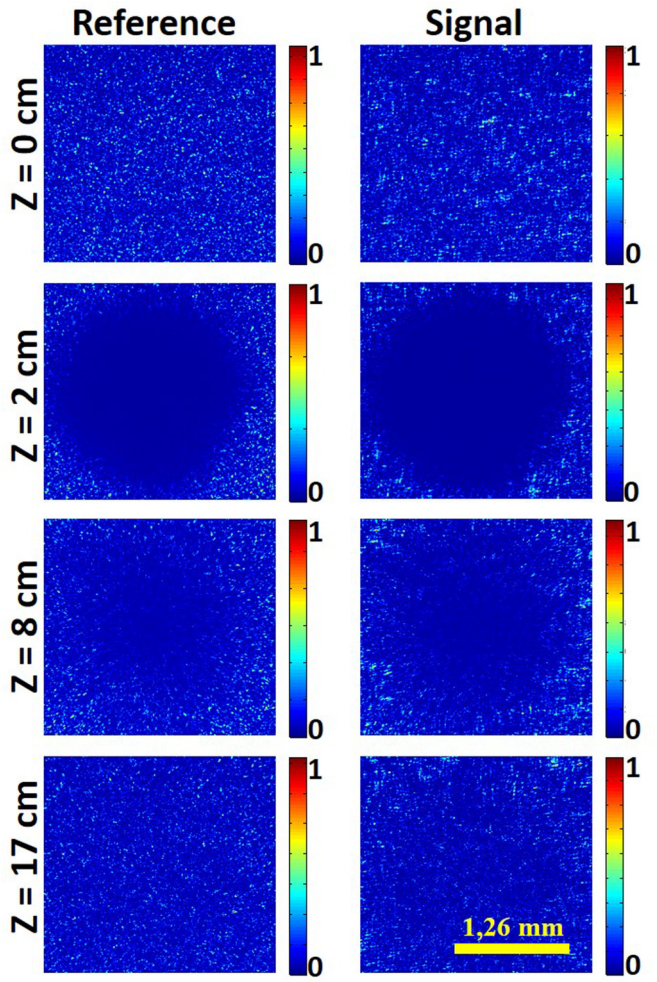

FIG. 4. Speckle patterns of the reference and signal beams measured for different distances of propagation, with spatial coherence length $\delta_2 = 17.7\ \mu$m and obstacle of diameter $D_1 \approx 2$ mm.

spot size of the laser beam over the RGGD, implies a reduction of the size of the image formed in the correlation function [25].

We use two parameters to evaluate the reconfiguration ability for the correlated imaging: the visibility and similarity. We have used the same experimental results shown in Figs. 3 and 5 to calculate the visibility and the similarity. The visibility

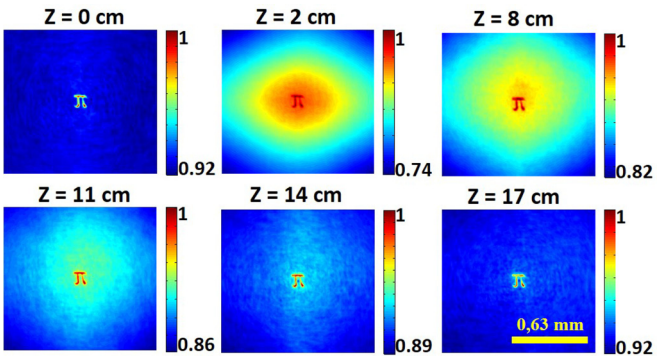

FIG. 5. Cross correlation between reference and signal beams for different distances of propagation, with coherence length $\delta_2 = 17.7\ \mu m$ and obstacle of diameter $D_1 = 2$ mm.

was calculated as the following:

$$V = \frac{I_L - I_B}{I_L + I_B}, \tag{12}$$

where I_L is the mean intensity of the pixels over the letter π and I_B is the mean intensity of the pixels out of the letter π (background). The similarity was calculated also using the data of Figs. 3 and 5, but following Ref. [26],

$$S = \frac{\iint I_f I_i dxdy}{\iint I_i^2 dxdy}, \tag{13}$$

where I_i is the intensity before the obstacle ($z = 0$ cm) and I_f are the intensities for the different propagation distances.

We have made a simulation to support the experimental results. Pseudorandom functions $R = R(x,y)$ are generated, such that each point assumes random values uniformly distributed between 0 and 2π. The speckle pattern is simulated by

$$P(x,y) = \mathbb{F}[A(x,y)e^{iR(x,y)}], \tag{14}$$

where $\mathbb{F}$ denotes a Fourier transform. The term $A(x,y)$ can be equal to $\exp[-(x^2+y^2)/w_1^2]$ for the reference beam or equal to a Fourier transform of a letter π for the signal beam. The result of Eq. (14) is assumed to correspond to

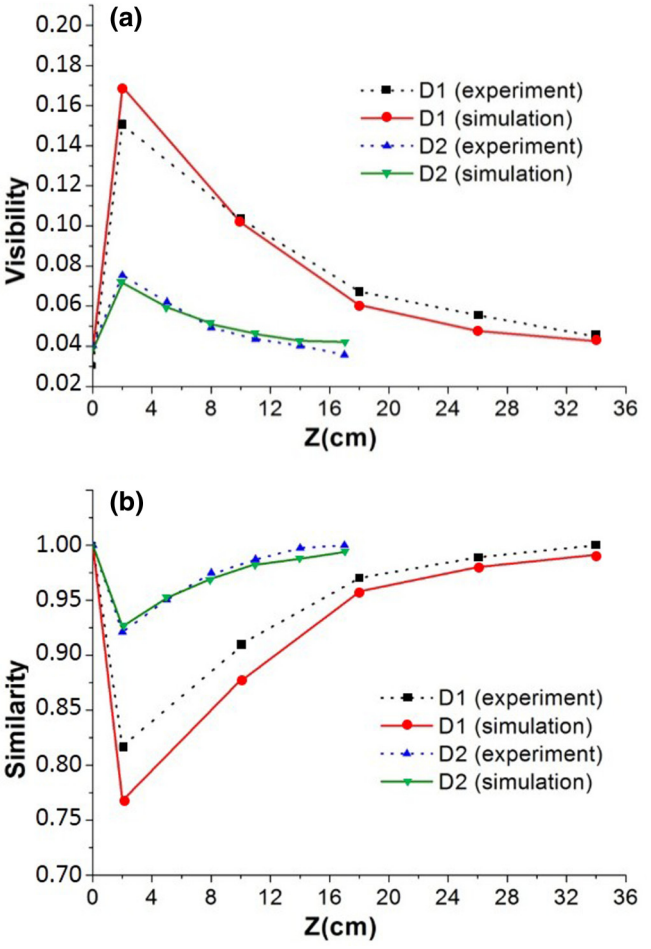

FIG. 6. Experimental and simulation results for visibility (a) and similarity (b) as a function of propagation distances for the spatial coherence length of $\delta_1 = 33.1\ \mu$m.

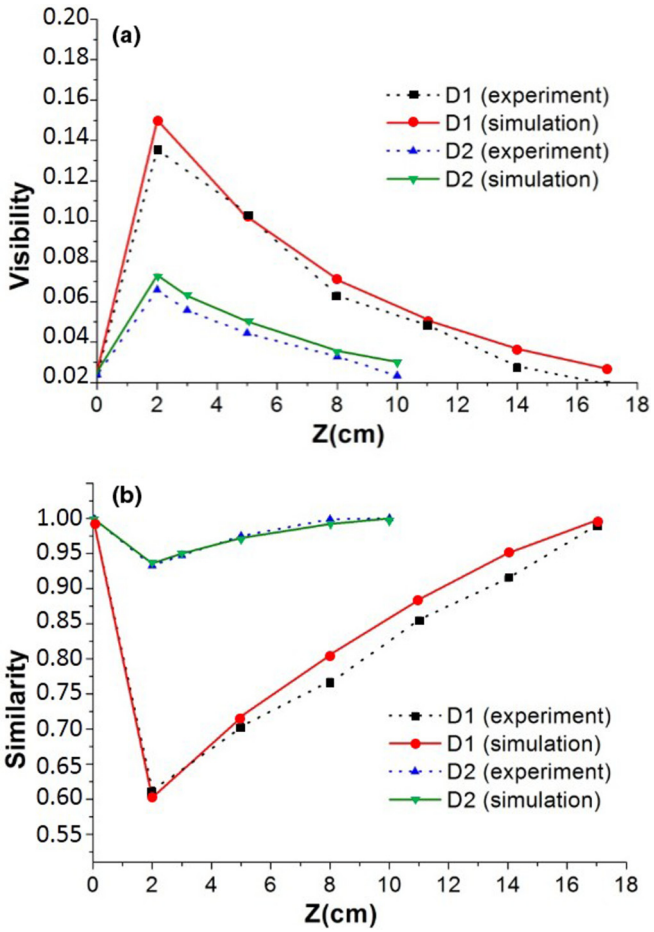

FIG. 7. Experimental and simulation results for visibility (a) and similarity (b) as a function of propagation distances for the spatial coherence length of $\delta_1 = 17.7\ \mu$m.

the plane at $z = 0$ cm. Adjusting w_1 we can control the spatial coherence length which is of the order of the speckle grain size. Next, we simulate the propagation of the signal and reference fields through the obstacle. After that, we numerically performed the cross correlation between the signal and reference intensities for the same distances of propagation presented in the experiments. All simulations have an average of 100 calculations. After obtaining a letter π similar to that in Figs. 3 and 5, we used Eqs. (12) and (13) to evaluate the visibility and similarity, respectively.

Figure 6 shows the visibility (a) and the similarity (b) for the cross-correlation images for different distances of propagation, corresponding to the numerical simulations and experimental results of Fig. (3). At $z = 2$ cm the visibility increases at the same time that similarity decreases. Along the propagation the visibility values decrease and return to a value close to one that it had before the obstacle, at $z = 0$ cm. Differently, the similarity values increase and approach to 1. It is important to point out that the similarity quantifies the reconfiguration effect, showing that the resolution of the letter π is recovered. It is interesting to notice that there is a trade-off between the visibility and the similarity, as observed in Fig. 6. This behavior can be also observed between visibility and resolution [27]. The resolution increases, while the visibility of the pattern decreases.

For a better understanding of the obstacle effect on visibility and similarity features, we performed the same study with an obstacle of diameter $D_2 \approx 1$ mm. As can be seen in Fig. 6, the insertion of the obstacle of minor diameter has less effect on the visibility and similarity, consequently reducing the reconfiguration distance. Thus, the visibility and similarity values return to those close to $z = 0$ cm at a propagation distance around $z = 17$ cm.

Figure 7 shows the visibility (a) and similarity (b) for the cross-correlation images along propagation, with the same parameters as Fig. 5, but now with spatial coherence length of $\delta_2 = 17.7\ \mu$m. For this case, the recovery of the visibility and similarity occurs at a shorter distance, since the reconfiguration distance is directly proportional to the coherence length [28].

It is remarkable that the correlated imaging is more robust against distortions during diffraction through obstacles when embedded in a more incoherent speckle pattern. All experimental results are in good agreement with the simulation.

We also should call attention to the fact that the speckles can be self-reconfigured independently if they were generated by partially coherent Gaussian or Bessel beams, for example [19].

V. CONCLUSION

In conclusion, we showed that an image, embedded into a speckle pattern, can be reconfigured after being transmitted by an object. This reconfiguration feature is quantified using the concepts of similarity and visibility. We observed that the insertion of an obstacle causes changes in these quantities, but they are reestablished during propagation, erasing completely any effect of the obstacle. We also observed that the propagation distance to recover the visibility and similarity depends on the spatial coherence length of the speckle and the obstruction size. The image reconfiguration using speckles may shed light in applications concerning microscopy in biological samples, since alternative avenues may be opened overcoming significantly the self-healing beams [17,18]. The self-reconfiguration effect also may be useful for entangled photons generated by a partially coherent pump [29,30].

ACKNOWLEDGMENTS

This work was supported by Coordenação de Aperfeiçoamento de Pessoal de Nível Superior (CAPES), Conselho Nacionalde Desenvolvimento Científico e Tecnológico (CNPq), Fundação de Amparo à Pesquisa do Estado de Alagoas (FAPEAL), and Instituto Nacional de Ciência e Tecnologia de Informação Quântica (INCT-IQ).

[1] D. M. Palacios, I. D. Maleev, A. S. Marathay, and G. A. Swartzlander, Jr., Phys. Rev. Lett. **92**, 143905 (2004).

[2] A. J. Jesus-Silva, J. M. Hickmann, and E. J. Fonseca, Opt. Express **20**, 19708 (2012).

[3] C. R. Alves, A. J. Jesus-Silva, and E. J. Fonseca, Optics Lett. **40**, 2747 (2015).
[4] J. Bertolotti, E. G. van Putten, C. Blum, A. Lagendijk, W. L. Vos, and A. P. Mosk, Nature **491**, 232 (2012).
[5] X. Yang, Y. Pu, and D. Psaltis, Opt. Express **22**, 3405 (2014).
[6] H. Yilmaz, E. G. van Putten, J. Bertolotti, A. Lagendijk, W. L. Vos, and A. P. Mosk, Optica **2**, 424 (2015).
[7] I. M. Vellekoop, A. Lagendijk, and A. P. Mosk, Nat. Photonics **4**, 320 (2010).
[8] E. G. van Putten, D. Akbulut, J. Bertolotti, W. L. Vos, A. Lagendijk, and A. P. Mosk, Phys. Rev. Lett. **106**, 193905 (2011).
[9] Y. Choi, T. D. Yang, C. Fang-Yen, P. Kang, K. J. Lee, R. R. Dasari, M. S. Feld, and W. Choi, Phys. Rev. Lett. **107**, 023902 (2011).
[10] O. Katz, E. Small, and Y. Silberberg, Nat. Photonics **6**, 549 (2012).
[11] S. M. Popoff, G. Lerosey, R. Carminati, M. Fink, A. C. Boccara, and S. Gigan, Phys. Rev. Lett. **104**, 100601 (2010).
[12] M. Kim, Y. Choi, C. Yoon, W. Choi, J. Kim, Q.-H. Park, and W. Choi, Nat. Photon. **6**, 583 (2012).
[13] H. Yu, T. R. Hillman, W. Choi, J. O. Lee, M. S. Feld, R. R. Dasari, and Y. K. Park, Phys. Rev. Lett. **111**, 153902 (2013).
[14] S. Popoff, G. Lerosey, M. Fink, A. C. Boccara, and S. Gigan, Nat. Commun. **1**, 81 (2010).
[15] J. Durnin, J. J. Miceli, and J. H. Eberly, Phys. Rev. Lett. **58**, 1499 (1987).
[16] G. A. Siviloglou and D. N. Christodoulides, Opt. Lett. **32**, 979 (2007).
[17] F. O. Fahrbach, P. Simon, and A. Rohrbach, Nat. Photonics **4**, 780 (2010).
[18] F. O. Fahrbach and A. Rohrbach, Nat. Commun. **3**, 632 (2012).
[19] C. R. Alves, A. J. Jesus-Silva, and E. J. S. Fonseca, Opt. Lett. **39**, 6320 (2014).
[20] J. P. Kirk and A. L. Jones, J. Opt. Soc. Am. **61**, 1023 (1971).
[21] J. D. Gaskill, *Linear Systems, Fourier Transforms, and Optics*, Wiley Series in Pure and Applied Optics (Wiley, New York, 1978).
[22] J. A. Newman and K. J. Webb, Opt. Lett. **37**, 1136 (2012).
[23] J. A. Newman and K. J. Webb, Phys. Rev. Lett. **113**, 263903 (2014).
[24] I. S. Reed, IRE Trans. Inf. Theory **8**, 194 (1962).
[25] F. Wang, X. L. Liu, Y. S. Yuan, and Y. J. Cai, Opt. Lett. **38**, 1814 (2013).
[26] X. X. Chu and W. Wen, Opt. Express **22**, 6899 (2014).
[27] I. Vidal, D. P. Caetano, E. J. S. Fonseca, and J. M. Hickmann, Opt. Lett. **34**, 1450 (2009).
[28] C. R. Alves, A. J. Jesus-Silva, and E. J. S. Fonseca (unpublished).
[29] A. K. Jha, G. A. Tyler, and R. W. Boyd, Phys. Rev. A **81**, 053832 (2010).
[30] M. McLaren, T. Mhlanga, M. J. Padgett, F. S. Roux, and A. Forbes, Nat. Commun. **5**, 3248 (2014).